

Dalton Transactions

Accepted Manuscript

This article can be cited before page numbers have been issued, to do this please use: M. Zienkiewicz, A. M. Jaboska-Wawrzycka, J. Szlachetko, Y. Kayser, K. Stadnicka, W. Sawka-Dobrowolska, J. Jezierska, B. Barszcz and J. Sa, *Dalton Trans.*, 2013, DOI: 10.1039/C3DT53288G.



This is an *Accepted Manuscript*, which has been through the RSC Publishing peer review process and has been accepted for publication.

Accepted Manuscripts are published online shortly after acceptance, which is prior to technical editing, formatting and proof reading. This free service from RSC Publishing allows authors to make their results available to the community, in citable form, before publication of the edited article. This *Accepted Manuscript* will be replaced by the edited and formatted *Advance Article* as soon as this is available.

To cite this manuscript please use its permanent Digital Object Identifier (DOI®), which is identical for all formats of publication.

More information about *Accepted Manuscripts* can be found in the [Information for Authors](#).

Please note that technical editing may introduce minor changes to the text and/or graphics contained in the manuscript submitted by the author(s) which may alter content, and that the standard [Terms & Conditions](#) and the [ethical guidelines](#) that apply to the journal are still applicable. In no event shall the RSC be held responsible for any errors or omissions in these *Accepted Manuscript* manuscripts or any consequences arising from the use of any information contained in them.

ARTICLE

Effective catalytic disproportionation of aqueous H₂O₂ with di- and mono-nuclear manganese(II) complexes containing pyridine alcohols ligands

Cite this: DOI: 10.1039/x0xx00000x

Received 00th January 2012,
Accepted 00th January 2012

DOI: 10.1039/x0xx00000x

www.rsc.org/

M. Zienkiewicz,^a A. Jabłońska-Wawrzycka,^a J. Szlachetko,^{b,c} Y. Kayser,^b K. Stadnicka,^d W. Sawka-Dobrowolska,^e J. Jezierska,^e B. Barszcz,^{*a} and J. Sá^{*b}

The two novel manganese(II) complexes with 2-hydroxymethylpyridine (2-CH₂OHpy) {[Mn₂(μ-Cl)₂(2-CH₂OHpy)₄]Cl₂·2H₂O (1)} and 2-hydroxyethylpyridine (2-(CH₂)₂OHpy) {[Mn(2-(CH₂)₂OHpy)₂(NCS)₂] (2)} were synthesized and characterized by means of X-ray diffraction, IR, EPR, HF EPR spectroscopy, magnetic and TG/DTG. The complexes show catalase-like activity in neutral aqueous solution since they were able to disproportionate H₂O₂ to harmless H₂O and O₂. Both complexes act as true catalysts since they reverted to their original form after depleting all the H₂O₂, as suggested by the operando resonant inelastic X-ray spectroscopy (RIXS) measurements.

Introduction

Catalases are enzymes that protect cells from deleterious effects caused by hydrogen peroxide. Besides heme-type catalases¹ and particular enzymes such as chloroperoxidase² that disproportionate hydrogen peroxide in addition to their peroxidase activity, there is a class of manganese catalases that can be found in bacterial organisms such as *Lactobacillus plantarum*³, *Thermus thermophilus*⁴, and *Thermoleophilum album*⁵. These enzymes are an extremely effective defence against 'oxidative stress' since they convert hydrogen peroxide into water and oxygen. They have been the motif of earlier structural and functional model research⁶. There is a need for low molecular weight enzymes models because natural enzymes revealed low effectiveness in clinical trials allegedly due to their low cell membrane permeability.

Manganese complexes are an important class of synthetic antioxidants^{6h-i,7}, inspired by natural enzymatic systems that contain this metal ion, which are able to neutralize reactive oxygen species (ROS). Previous reports were focused on the synthesis of the dimmeric manganese complexes containing manganese ions in +II and +III oxidation states as catalase mimics systems^{6h-i,7}. Our work concerns the synthesis of structurally different dimmeric, monomeric and polymeric compounds, containing manganese ions in the +II oxidation state. We have found earlier that the complex [Mn(2-CH₂OHpy)(SO₄)(H₂O)]_n (2-CH₂OHpy = 2-

hydroxymethylpyridine)⁸ could be a good low molecular weight model for manganese catalase because it was able to disproportionate H₂O₂ to H₂O and O₂ in neutral aqueous conditions, which is an uncommon case among synthetic antioxidants, known to display high activity in organic solvents⁹ but extremely low reactivity or even none in aqueous solutions with a pH < 8 (physiological pH values). Furthermore, the manganese(II) polymeric complex [Mn(2-CH₂OHpy)(SO₄)(H₂O)]_n was found to be stable and catalytic by means of resonant inelastic scattering spectroscopy (RIXS).

There is an appreciable interest in pyridine-based chelating alcohols that are widely used in coordination chemistry due to the presence of ligands containing N,O-donor atoms, which can be adopted to modeling coordination environments of synthetic analogues that mimic both the structure and function of the active sites of metal enzymes. Based on the results above our approach was to design a highly active structurally various manganese(II) complexes with homologous of pyridine alcohols with different counter-ions and compare their catalytic activity.

Herein, we report the synthesis and full physical characterization of two novel manganese(II) complexes with 2-hydroxymethylpyridine (2-CH₂OHpy) {[Mn₂(μ-Cl)₂(2-CH₂OHpy)₄]Cl₂·2H₂O (1)} and 2-hydroxyethylpyridine (2-(CH₂)₂OHpy) {[Mn(2-(CH₂)₂OHpy)₂(NCS)₂] (2)}. The catalytic activity of the complexes in the presence of H₂O₂ in aqueous solution was evaluated and the evolution of molecular

oxygen was monitored by a quadrupole mass-spectrometer (QMS). RIXS measurements depicted the involvement of manganese +II and +III oxidation states in the reaction. The complexes reverted to their original form after H_2O_2 depletion, which confirms these systems as truly catalytic process. In addition, the presented catalytic activity of Mn-model complexes may also provide valuable scientific background information for green chemistry¹⁰ and cancer therapy due to the fact that cellular levels of H_2O_2 directly or indirectly play a key role in malignant transformation and sensitize cancer cells to death¹¹.

Results and discussion

We synthesised two novel manganese(II) complexes that can mimic catalytic properties of manganese catalase, namely $[\text{Mn}_2(\mu\text{-Cl})_2(2\text{-CH}_2\text{OHpy})_4]\text{Cl}_2 \cdot 2\text{H}_2\text{O}$ (**1**) (Fig. 1) and $[\text{Mn}(2\text{-CH}_2\text{OHpy})_2(\text{NCS})_2]$ (**2**) (Fig. 2), and characterized using X-ray diffraction, IR, EPR, HF EPR spectroscopy, magnetic and TG/DTA data. The catalytic activity of synthesized complexes was evaluated by monitoring the oxygen evolution with a QMS, and the changes in the catalysts metal centre were determined by RIXS.

Manganese(II) complexes with pyridine alcohols characterization

Crystal and refinement data of compounds **1** and **2** are listed in Table 1. According to the crystallographic analysis, the molecular structure of $[\text{Mn}_2(\mu\text{-Cl})_2(2\text{-CH}_2\text{OHpy})_4]\text{Cl}_2 \cdot 2\text{H}_2\text{O}$ (**1**) consists of two centro-symmetrically related Mn(II) centres bridged by two chloride ions. Mn(1)-Cl(1)-Mn(1)ⁱ-Cl(1)ⁱ atoms form a square with a centre of inversion (Fig. 1). The Mn(II) ion is surrounded by two chelating 2-CH₂OHpy molecules bonded through N and O atoms (Mn(1)-N(2A) = 2.2309(1) Å; Mn(1)-N(2B) = 2.2273(1) Å; Mn(1)-O(8A) = 2.2143(1) Å; Mn(1)-O(8B) = 2.1912(1) Å). The two coordinated bridging chlorides, with distances of 2.5065(5) and 2.5280(5) Å, are nearly symmetrical, and the Mn-Cl-Mn bridging angle is 92.81°. The shape of the polyhedra is irregular and does not assume octahedral geometry because possesses only the identity symmetry. The other two chloride ions act as counterions. The Mn...Mn distance is equal to 3.646(5) Å, which is much shorter than that for Cu centres in the dimeric structure of another 2-CH₂OHpy complex¹². Selected geometrical data for **1** are given in Table 2.

The crystal structure of **1** is stabilised by two types of hydrogen bonds: O-H...O and O-H...Cl (Fig. 3, Table 3). Intramolecular interactions involve the oxygen atoms O(8A) and O(8B) of the hydroxymethyl group of 2-CH₂OHpy as donors and the oxygen atom O(1W) of water molecule or a non-coordinated chloride ion Cl(2) as an acceptor, respectively. Two non-coordinated chloride ions involved in the formation of H-bonds with two water molecules form a system with a centre of inversion within the unit cell. The intermolecular $\pi\cdots\pi$ interactions between the parallel-displaced pyridine rings of two neighbouring complex molecules contribute also to the

structural stabilisation (Table 4, Fig. 3). The Cg01-Cg01(-x+1, -y, -z+1) centroid distance is approximately 3.654 Å. This distance is slightly shorter than that for a cadmium complex (3.796 Å) with the same ligand¹³.

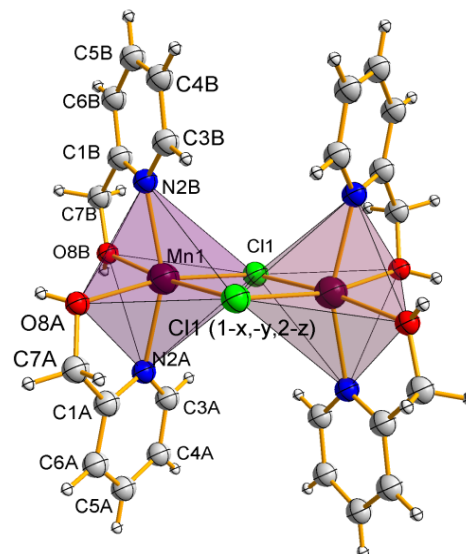


Fig. 1 Molecular structure with the atom numbering scheme and coordination polyhedron of complex **1**.

Table 1 crystal data and structure refinement for **1** and **2**

	1	2
Empirical formula	$\text{C}_{24}\text{H}_{32}\text{N}_4\text{O}_6\text{Cl}_4\text{Mn}_2$	$\text{C}_{16}\text{H}_{18}\text{N}_4\text{O}_2\text{S}_2\text{Mn}$
Formula weight	724.22	417.40
Temperature (K)	293(2)	100(2)
Crystal system, space group	triclinic, $P\bar{1}$	monoclinic, $P2_1/c$
Unit cell dimensions		
<i>a</i> (Å)	7.8970(2)	8.778(1)
<i>b</i> (Å)	9.7655(3)	14.298(2)
<i>c</i> (Å)	11.4184(4)	7.848(1)
α (°)	73.570(2)	90.00
β (°)	70.964(2)	112.71(1)
γ (°)	77.267(2)	90.00
Cell volume (Å ³)	790.41(4)	908.68(2)
<i>Z</i>	1	2
Crystal size (mm)	0.40 × 0.23 × 0.15	0.23 × 0.21 × 0.15
θ range (°)	3.08–27.50	2.89–27.98
Calculated density (gcm ⁻³)	1.521	1.526
Limiting indices	$-10 \leq h \leq 9, -12 \leq k \leq 12, -14 \leq l \leq 11$	$-10 \leq h \leq 11, -18 \leq k \leq 18, -10 \leq l \leq 10$
Absorption coefficient (mm ⁻¹)	1.179	0.973
Absorption correction	Semi-empirical from equivalents	Analytical
T_{max} and T_{min}	0.8429 and 0.6429	0.901 and 0.846
Reflections collected/unique/observed	3551/2986	2166/1669
$[I > 2\sigma(I)]$	$[R_{\text{int}} = 0.0191]$	$[R_{\text{int}} = 0.0310]$
Data/parameters	3551/194	1669/127
Goodness-of-fit on F^2	0.875	0.936
Final <i>R</i> indices $[I > 2\sigma(I)]$	$R_1 = 0.0270,$ $wR_2 = 0.0695$	$R_1 = 0.0386,$ $wR_2 = 0.0920$
<i>R</i> indices (all data)	$R_1 = 0.0356,$ $wR_2 = 0.0736$	$R_1 = 0.0553,$ $wR_2 = 0.0966$
Largest differences in peak and hole (e Å ⁻³)	0.250 and -0.263	0.465 and -0.296

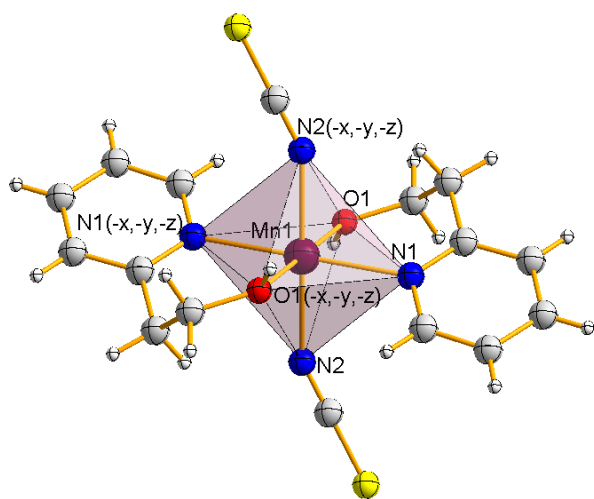


Fig. 2 Molecular structure with the atom numbering scheme and coordination polyhedron of complex **2**.

Table 2 Selected bond lengths (Å) and valence angles (°) for **1** and **2**

Compound 1

Bond lengths (Å)			
Mn(1)-N(2A)	2.2309(1)	Mn(1)-N(2B)	2.2273(1)
Mn(1)-O(8A)	2.2143(1)	Mn(1)-O(8B)	2.1912(1)
Mn(1)-Cl(1)	2.5065(5)	Mn(1)-Cl(1) ⁱ	2.5280(5)
Valence angles (°)			
O(8B)-Mn(1)-O(8A)	91.82(5)	O(8B)-Mn(1)-Cl(1) ⁱ	172.94(3)
O(8B)-Mn(1)-N(2B)	72.50(5)	O(8A)-Mn(1)-Cl(1) ⁱ	87.68(4)
O(8A)-Mn(1)-N(2B)	92.64(5)	N(2B)-Mn(1)-Cl(1) ⁱ	100.48(4)
O(8B)-Mn(1)-N(2A)	90.63(5)	N(2A)-Mn(1)-Cl(1) ⁱ	95.98(4)
N(2B)-Mn(1)-N(2A)	158.26(5)	N(2B)-Mn(1)-Cl(1)	98.97(4)
O(8B)-Mn(1)-Cl(1)	94.58(4)	Cl(1)-Mn(1)-Cl(1) ⁱ	87.191(1)
O(8A)-Mn(1)-Cl(1)	168.00(3)	N(2A)-Mn(1)-Cl(1)	95.91(4)
O(8A)-Mn(1)-N(2A)	73.85(5)		

Compound 2

Bond lengths (Å)			
Mn(1)-O(1)	2.2020(16)	Mn(1)-N(2)	2.2069(19)
Mn(1)-N(1)	2.2463(18)		
Valence angles (°)			
O(1) ⁱ -Mn(1)-O(1)	180.00	N(2)-Mn(1)-N(1) ⁱ	94.18(7)
O(1)-Mn(1)-N(2) ⁱ	91.08(7)	O(1)-Mn(1)-N(1)	85.35(6)
O(1)-Mn(1)-N(2)	88.92(7)	N(2)-Mn(1)-N(1)	85.82(7)
N(2)-Mn(1)-N(2) ⁱ	180.00	N(1)-Mn(1)-N(1) ⁱ	180.00

Symmetry codes: **1** (i) $-x+1, -y+2, -z$; **2** (i) $-x, -y, -z$.

Molecular structure of **2** is best represented by the formula $[\text{Mn}(\text{2-(CH}_2)_2\text{OHpy})_2(\text{NCS})_2]$, and structure of the complex is shown in Fig. 2. Selected bond distances and bond angles values are listed in Table 2. In the symmetric manganese complex $[\text{Mn}(\text{2-(CH}_2)_2\text{OHpy})_2(\text{NCS})_2]$ a Mn^{II} ion is located on the centre of symmetry and the octahedral environment provided by one $\text{2-(CH}_2)_2\text{OHpy}$, one SCN^- and their symmetry related counterparts. Thus, the Mn center is surrounded by two nitrogen from the SCN^- anions ($\text{Mn(1)-N(2)} 2.2069(19) \text{ \AA}$) and two nitrogen and two oxygen from the chelating $\text{2-(CH}_2)_2\text{OHpy}$ ligands ($\text{Mn(1)-N(1)} 2.2463(18) \text{ \AA}$, $\text{Mn(1)-O(1)} 2.2020(16) \text{ \AA}$) that form an almost perfect octahedron with angular deviations smaller than 5° . Distances and angles within the coordination environment of Mn^{II} are in agreement with the distances found in the literature for similar compound¹⁴.

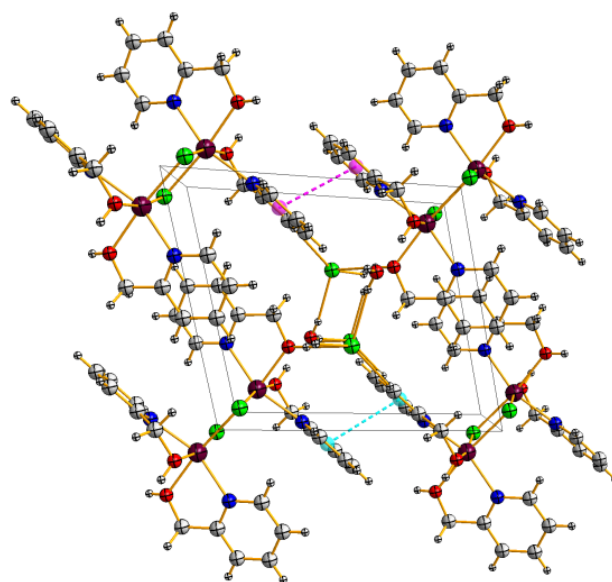


Fig. 3 Crystal packing of **1** with marked H-bonds $\text{O-H}\cdots\text{O}$ and $\text{O-H}\cdots\text{Cl}$ type and $\pi\cdots\pi$ interactions viewed along $[1\ 0\ 0]$ direction.

Table 3 Hydrogen bonds for complexes **1** and **2** (Å) and (°)

Compound 1

D-H...A	d(D-H)	d(H...A)	d(D...A)	<DHA
O(1W)-H(1W1)...Cl(2) ⁱ	0.85(3)	2.33(1)	3.155(2)	163(3)
O(1W)-H(1W2)...Cl(2)	0.85(3)	2.32(1)	3.153(2)	169(3)
O(8A)-H(8A)...O(1W) ⁱⁱ	0.85(3)	1.77(1)	2.614(2)	173(2)
O(8B)-H(8B)...Cl(2)	0.85(3)	2.15(1)	3.002(1)	175(2)

Compound 2

D-H...A	d(D-H)	d(H...A)	d(D...A)	<DHA
O(1)-H(1)...S(1) ⁱ	0.76(3)	2.43(3)	3.1612(2)	162(3)
C(7)-H(7)...N(2) ⁱⁱ	0.97	2.57	3.356(3)	138

Symmetry codes: **1** (i) $-x+2, -y+1, -z+1$, (ii) $x-1, y, z$; **2** (i) $x, -y+0.5, z+0.5$, (ii) $-x, -y, -z$.

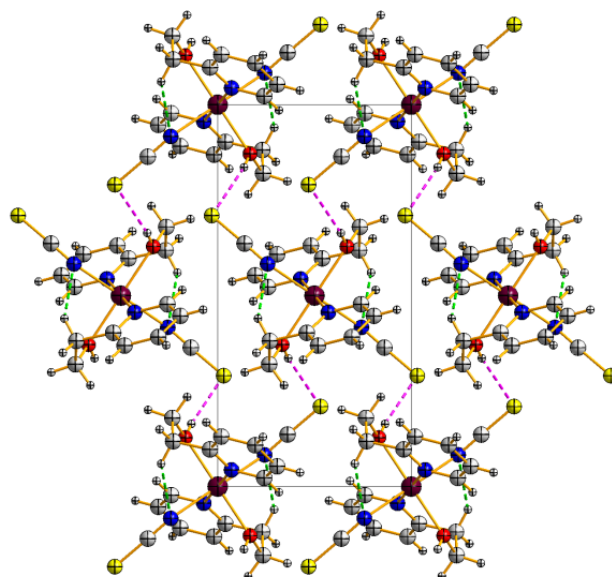


Fig. 4 View of a 1D supramolecular network of complex **2**. View along $[1\ 0\ 0]$ direction.

Table 4 $\pi \cdots \pi$ interactions for **1** and **2** (Å)

	$\pi \cdots \pi$	d(Cg \cdots Cg) (Å)	offset
1	Cg01-Cg01 _(-x+1, -y, -z+1)	3.654	1.435
2	Cg-Cg _(-x+1, -y, -z)	3.598(2)	1.105

Compound **1**: Cg01, N(2A)-C(6A), compound **2**: Cg, N(1)-C(6)

Analysis of the crystal structure at the supramolecular level reveals that the complex molecules are held together by one intermolecular O(1)-H(1) \cdots S(1)ⁱ hydrogen bond and one weak C(7)-H(7) \cdots N(2)ⁱⁱ intramolecular interaction. (Table 3). These interactions define a 1D structure running along [1 0 0] (Fig 4), and intermolecular $\pi \cdots \pi$ stacking interactions (Table 4) between centrosymmetric molecules of pyridine ring. The mean intercentroid and interplanar distances between aromatic rings (3.598(2) Å and 3.424(2) Å; symmetry code $-x+1, -y, -z$) corresponds well with the relative parameter found in structures of metal complexes with aromatic nitrogen-containing ligands.

The IR spectra confirmed the results of the X-ray studies with respect to the N, O-donor type of coordination of both ligands. The electron – donating capabilities of the homologous pyridine alcohols: 2-CH₂OHpy and 2-(CH₂)₂OHpy can be estimated by comparing the OH stretching vibration of the –CH₂OH and –(CH₂)₂OH groups and the C=N frequencies of the pyridine ring of Mn^{II} complexes (**1**, **2**) with those of the free ligands, respectively. Both organic molecules exhibit broad absorption bands at 3300–3500 cm⁻¹, which are assigned to intramolecular hydrogen bond $\nu(\text{O-H}\cdots\text{N})$ vibration^{14a,15}. The complexes formation leads to hampering this proton exchange, which results in one absorption band for each complex shifted towards higher energies. On the coordination of homologous pyridine alcohols with Mn^{II} ions the $\delta\text{C-O}$ bands are shifted to higher wavenumbers compared to free ligands ($\Delta = 5$ cm⁻¹ for **1** and $\Delta = 9$ cm⁻¹ for **2**), which confirms the expected M–O coordination. Additionally, the $\nu\text{C=N}$ frequencies of the pyridine ring are shifted by 12 cm⁻¹ and 7 cm⁻¹ for **1** and **2**, respectively. These shifts are correlated with the binding mode of these ligands, which are sensitive to manganese coordination through the nitrogen atom from pyridine ring and also *via* the oxygen atom of the –CH₂OH or –(CH₂)₂OH groups. Moreover, the IR spectra of **1** and **2** show new bands that are attributed to chloride and thiocyanate ions in the coordination sphere of the complexes. Two new bands for νCl^- at 686 and 644 cm⁻¹ in complex **1** indicate the presence of chlorides in the structure. The strong new band at 2079 cm⁻¹ in **2** can be assigned to the νNCS^- of the thiocyanate ion.

The room temperature magnetic moment of powdered sample of monomeric complex **2** is 5.58 B.M. The calculated value of μ_{eff} was similar to those observed for the five uncoupled spins ($S = 5/2$, 5.92 B.M.) of Mn(II)¹⁶. This contrasts to the dinuclear complex **1**, in which magnetic moments decreased when temperature was lowered, especially below 50 K. This behavior was interpreted in terms of HDVV Hamiltonian, $H = -J \hat{S}_1 \cdot \hat{S}_2$, where $S_1 = S_2 = 5/2$ ^{17b,e,h,18}. The temperature dependence (in the range 1.8 – 300 K) of the molar

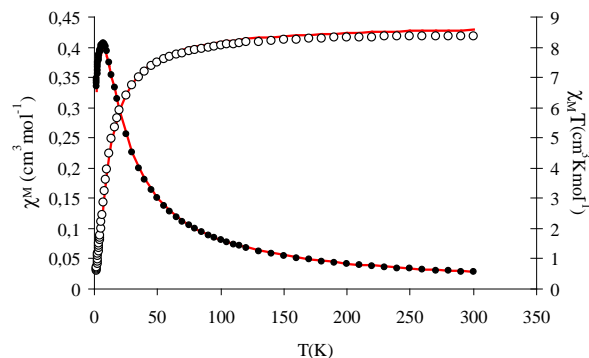


Fig. 5 The temperature dependence of χ_M (•) and $\chi_M T$ (○) for **1**. The solid red lines result from the best least-squares fit using the parameters described in the text.

magnetic susceptibility χ_M as well as $\chi_M T$ shown in Fig. 5 was analyzed according to equation 1:

$$\chi = \frac{2Ng^2\beta^2}{kT} \frac{e^x + 5e^{3x} + 14e^{6x} + 30e^{10x} + 55e^{15x}}{1 + 3e^x + 5e^{3x} + 7e^{6x} + 9e^{10x} + 11e^{15x}} \quad \text{Eq. 1}$$

where $x = J/kT$.

The best least-squares fitting of the experimental magnetic data using this equation leads to $g = 2.00$ and $J = -1.63$ cm⁻¹ with very good agreement factor $R = 2.8 \times 10^{-4}$. The negative J value indicates weak but distinct antiferromagnetic coupling in compound **1**.

The magnetic interactions in Mn(II) compounds with double-chloride bridges are very sensitive to the structural parameters (distances and angles) of $\{\text{Mn}_2(\mu\text{-Cl})_2\}^{2+}$ core¹⁷, which is directly related to the space group of monocrystals collected in Table 5. For these complexes, which are antiferromagnetically or ferromagnetically coupled, we try to find some magneto-structural correlation (Fig. S1). The correlation between J values and Mn-Cl-Mn angles presented in Fig. S1a indicates that the ferromagnetic interactions between two manganese(II) ions increases with the increase of the Mn-Cl-Mn angle. Furthermore, the linear regression in Fig. S1a calculated from the geometrical data predicts a change from antiferromagnetic to ferromagnetic behaviour at angle value of 95°. On the other hand the relationship between the measured Mn \cdots Mn distance values and their magnetic exchange coupling constant (J) predicts the crossover from anti- to ferromagnetic interactions at about 3.76 Å (Fig. S1b).

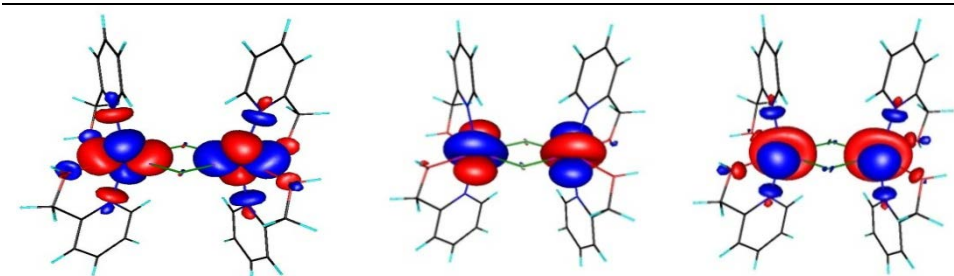
Basing on plots in Fig. S1, and despite the existing correlation between J and the Mn-Cl-Mn angle ($R = 0.8125$ or including only dimers: $R = 0.8848$) and Mn \cdots Mn distance ($R = 0.7830$), the complexes **I** and **II** exhibit antiferromagnetic exchange whereas complex **X** exhibit ferromagnetic exchange, when their geometrical parameters are taken into account. These deviations suggest that some differences between the theoretical predictions and the experimental findings occur. In addition, the structural dependence of magnetic interaction between Mn^{II} centres may also be referred to donor properties and the structure of chelating ligands around the metal ion. The

Table 5 Comparison of the structural parameters (distances (Å) and angles (°)) and magnetic interaction (J (cm⁻¹), based on the Spin Hamiltonian $-J \hat{S}_1 \hat{S}_2$) for dinuclear and polynuclear complexes with a {Mn₂(μ-Cl)₂}²⁺ core

No	Compound ^a	Space group	α (Mn-Cl-Mn) (°)	d(Mn-Cl) (Å)	d(Mn...Mn) (Å)	J (cm ⁻¹)	Interactions	Ref.
I	[MnCl(pyz)(H ₂ O)] _n	C2/c	93.36(2)	2.4837(8)	3.664(4)	+0.42	weak ferromagnetic	17a
II	[Mn(μ-Cl)(biz) ₂ Cl ₂]	$P \bar{1}$	93.53(4)	2.5513(8) 2.5757(1) 2.5578(1)	3.740	+0.33(1)	weak ferromagnetic	17b
III	[Mn ₂ (dpp) ₂ (H ₂ O) ₂ Cl ₄]2H ₂ O	$P2_1/c$	95.68(7)	2.523(2) 2.610(2)	3.805(2)	+0.11	weak ferromagnetic	17c
IV	[Mn(μ-Cl) ₂ (phen)] _n	C2/c	96.06(6)	2.4821(2) 2.6499(2)	3.817	+0.017	weak ferromagnetic	17d
V	[(μ-Cl) ₂ MnL ² (PF ₆) ₂]	$P2_1/n$	95.52(2)	2.4915(6) 2.5408(6)	3.726	+1.49	ferromagnetic/ antiferromagnetic	17e
VI	[Mn(μ-Cl) ₂ (mppma)] _n	$P2_1/c$	94.137(2)	2.5811(6) 2.5265(6)	3.7398(4)	-0.255(0)	weak antiferromagnetic	17f
VII	[Mn(4-CNpy) ₂ Cl ₂]	$P2_1/c$	93.5	2.525(2) 2.555(2)	3.700	-0.792(6)	antiferromagnetic	17g
VIII	[TPA ₂ Mn ₂ (μ-Cl) ₂] ²⁺	$P2_1/c$	<90	2.4056(9) 2.6286(1)	3.521(2)	-8.8	antiferromagnetic	17h
IX	[Mn(μ-Cl) ₂ (bpy)] _n	$I2/a$	96.4	2.4813(1) 2.6616(1)	3.8352(7)	+0.19	weak ferromagnetic	17i-j
X	[{MnCl((-)-L)} ₂ (μ-Cl) ₂]	$P2_1$	95.91(5)	2.5772(1) 2.4356(1)	3.736	-0.22	weak antiferromagnetic	17k
XI	[{Mn(mpbpa)Cl} ₂ (μ-Cl) ₂]	$P2_1/c$	96.426(2)	2.5684(6) 2.5950(6)	3.8500(6)	+1.10	ferromagnetic	17l
XII	[{Mn(bpea)Cl} ₂ (μ-Cl) ₂]	$P2_1/c$	95.72(2)	2.5374(9) 2.5683(7)	3.786	+0.68	ferromagnetic	17m
	1	$P \bar{1}$	92.81(2)	2.507(2) 2.528(4)	3.646(5)	-1.63	antiferromagnetic	this work

aAbbreviations: pyz = 2-pyrazinecarboxylate, biz = 2,2-bi-imidazole, dpp = 2,3-bis(2-pyridyl)pyrazine, phen = 1,10-phenanthroline, L² = N,N'-bis(2-pyridylmethylene)propanediamine, mppma = N-(3-methoxypropyl)-N-(pyridin-2-ylmethyl)amine, 4-CNpy = 4-cyanopyridine, TPA = tris(2-pyridylmethyl)amine, bpy = 2,2'-bipyridine, (-)-L = (-)-pinene[5,6]bipyridine, mpbpa = N-(3-methoxypropyl)-N,N-bis(pyridin-2-ylmethyl)amine, bpea = N,N-bis(2-pyridylmethyl)ethylamine

Table 6 The calculated singly occupied natural orbitals of **1** for $S_1 = S_2 = 5/2$

			Orbital (occup. number)	Overlap
153			152	0.05590
154			155	0.01455
152			153	0.02727
			154	0.02526
			156	0.01290

preparation and study of additional systems of this category will play an instrumental role in confirming the trends observed here.

The value of exchange integral was also calculated at DFT level by using the “broken symmetry” method. The predicted J value is -3.4 cm⁻¹ that satisfactory reproduces the experimental value. The quality of the DFT prediction of J value is in our opinion reasonable, taking into account that theoretically predicted exchange integrals of small values are usually twice greater than experimental¹⁹. It seems to be specially important that the result of DFT calculations theoretically supports an antiferromagnetic character of the exchange interactions. They are illustrated by the diagrams of three from five Mn^{II} d-orbitals participating in weak metal-metal interactions are shown in

Table 6; the calculated magnetic orbitals at separate Mn^{II} ions suggest that dx²-y² orbital in 153 and dz² orbital in 154 and 152 are dominant.

The X-band EPR spectra of powdered compounds **1** and **2** at 77 K are shown in Fig. 6. For monomeric complex **2** the spectrum exhibits fine structure signals resulting from ZFS of the spin states for the high-spin d⁵ metal ion. It can be parameterized using the following Spin Hamiltonian:

$$H = \beta Sg B + D[S_z^2 - 1/3S(S+1)] + E(S_x^2 - S_y^2) \quad \text{Eq. 2}$$

where $S = 5/2$ and D and E are ZFS parameters for individual Mn^{II} ion representing the axial and rhombic parts, respectively. The simulation of the experimental spectrum for **2**, using a

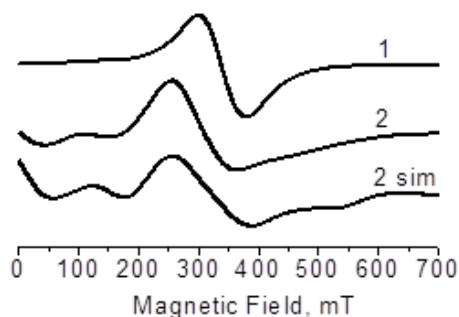


Fig. 6 X-band EPR spectra of powdered compounds **1** and **2** at 77 K, together with the spectrum for **2** (sim **2**) simulated with the spin Hamiltonian parameters given in the text.

computer program SPIN²⁰ gave the approximate spin Hamiltonian parameters, $g = 2$, $D = 0.089 \text{ cm}^{-1}$ and $E = 0.023 \text{ cm}^{-1}$. The parameters are close to those estimated from the EPR spectra with similar fine structure signals for other Mn^{II} complexes forming the distorted polyhedra²¹, especially for octahedral Mn^{II} and seven-coordinated Mn^{II} with N₃O₄ donor set ($D = 0.086 \text{ cm}^{-1}$, $E = 0.026 \text{ cm}^{-1}$)²².

Dinuclear compound **1** exhibits a characteristic broad line with $g_{\text{eff}} = 2.03$, what precludes finding of the zero field splitting parameters. Hence, we carried out the measurements at 224 GHz and 5 K for dinuclear compound **1**. Unfortunately, the interpretation of the obtained spectrum (Fig. 7), consisting of large amount of the signals from the resonance transitions within most likely very complicated system of energy levels, appeared to be practically impossible. Only the D_{dip} contribution to D_{12} in Mn^{II} dimer due to the dipole-dipole interaction of unpaired electrons was estimated. It equals $-3g^2\mu_B^2/r^2$ giving $-0.107(2) \text{ cm}^{-1}$ for $r(\text{Mn-Mn}) = 3.646 \text{ \AA}$.

The thermal data correlates well with the molecular structure of both compounds. The fragments of ligands containing N, O-donor atoms decomposed during the last stages. The detailed results of the TG/DTG analyses of **1** and **2** are listed in Fig. S2.

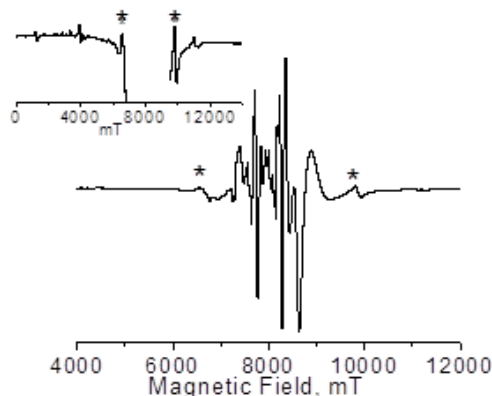


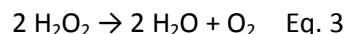
Fig. 7 The EPR spectrum of the powdered compound **1** at 224 GHz and 5 K; in inset the amplified signals on left and right from the asterisks are presented.

The TG curve of complex **1** exhibits seven decomposition steps (Fig. S2a). The two molecules of lattice water (4.24%) are released in the temperature range of 70 to 140 °C. Endothermic effects (max. 93 °C) are observed in the DSC curve (Fig. S2c). In the second step, compound **1** loses fragments of organic ligands and a Cl₂ molecule (from non-coordinated chloride ions). The next four steps over the temperature range of 195 to 500 °C correspond to the loss of parts of the four pyridine rings (37.80%). The last stage is described by a mass loss of 12.99% and is accompanied by the final fragmentation of organic ligand molecules containing N-donor atoms and a Cl₂ molecule from the double chloride bridges. A residue of MnO₂ remains.

Decomposition process of **2** proceeded in three main stages over the temperature range of 90 to 1000 °C (Fig. S2b). The first step begins at 90 °C and is attributed to the elimination of the 2-(CH₂)₂OHpy molecules fragments (44.15%). In the second stage, up to 255 °C, a CS₂ molecule from thiocyanate ligand is released (18.24%). The successive mass loss (16.79%) from 405 to 1000 °C may be attributed to the final decomposition of two organic ligands and thiocyanate ions, leading to MnO₂ formation.

Catalase-like activity of complexes **1** and **2** and RIXS measurements

The synthesized complexes catalytic activity was tested in H₂O₂ disproportionation. According to catalytic activity of this metalloenzyme, hydrogen peroxide is destroyed resulting in the formation of oxygen and water in the reaction (Eq. 3):



The oxygen evolution for both compounds is depicted in Fig. 8. The average oxygen evolution achieved with dimmeric complex **1** was ca. $414.8 \text{ cm}^3(\text{min} \cdot \text{mol}_{\text{cat}})^{-1}$, which is significantly higher than with monomeric complex **2** (ca. $35.6 \text{ cm}^3(\text{min} \cdot \text{mol}_{\text{cat}})^{-1}$). Even if the results are normalized to Mn content, the complex **1** is still roughly eight times more active than **2**. The result suggests that the monomeric complex **2** needs to find a second complex in order to react, similarly to what was published elsewhere⁸, and catalytic activity increases if they are in close proximity like in the case of dimmeric complex. It should be mentioned that both complexes are significantly more active than the one published by Zienkiewicz et al.⁸ since reaction was completed within 2-3 h.

Mn K-edge RIXS maps were collected to determine the electronic structure of the metal center, in particular the p-orbital contribution to the unoccupied orbitals²³, which are involved in chemical reaction²⁴. The RIXS maps of complex **1** prior, during and after reaction are depicted in Fig. 9. The RIXS map of **1** in water is dominated strong absorption around 6551-6552 eV, which is similar to the RIXS map of solid complex. Therefore the signal can be ascribed to Mn^{II}²⁵. The addition of H₂O₂ led to a significant increase in the absorption, i.e., decrease in the occupancy of the p-states that is consistent with increase of oxidation state from +II to +III. The RIXS map of **1** after reaction completion was similar to complex in water.

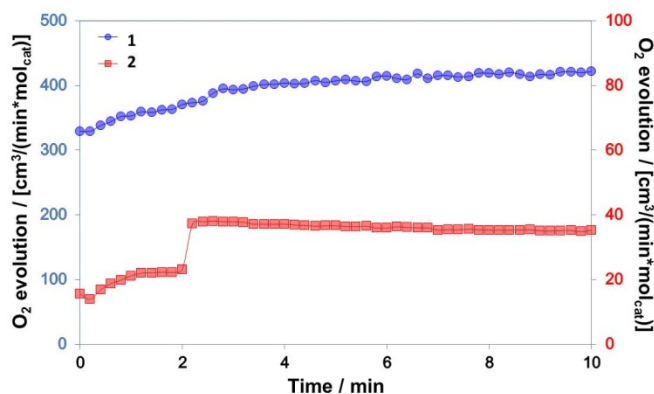


Fig. 8 Oxygen evolution from the disproportionation of H_2O_2 in the presence of **1** (blue) and **2** (red) in water at 22 °C.

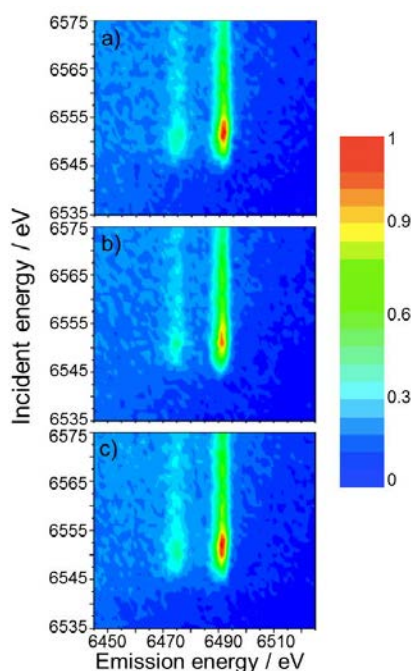


Fig. 9 RIXS maps of **1** a) in water; b) during reaction (water + H_2O_2); and c) after reaction.

The RIXS results suggest that Mn redox chemistry is directly involved in the catalytic reaction, and the reaction with dimeric complex **1** is in fact catalytic not stoichiometric.

Similar strategy was used to evaluate Mn oxidation state on complex **2**. The RIXS maps of **2** prior, during and after reaction are depicted in Fig. 10. As with dimeric complex **1**, the RIXS map shows a strong absorption at 6551–6552 eV, which was also present in the solid form of the complex. Therefore the oxidation state of Mn is +II prior to reaction. The addition of H_2O_2 resulted in a significant increase in the absorption intensity, reflecting an increase of the unoccupied p-states, which is synonymous of increase of Mn oxidation state from +II to +III. RIXS map after reaction is similar to the one in water (prior to reaction). Therefore, as with the case of **1** RIXS maps confirmed that redox chemistry of Mn are directly

involved in the catalytic cycle and the system is in fact catalytic. RIXS experiments indicate that both complexes follow the mechanism proposed elsewhere⁸, suggesting that Mn (+II) is not only the final oxidation state but also necessary for a new catalytic cycle to take place.

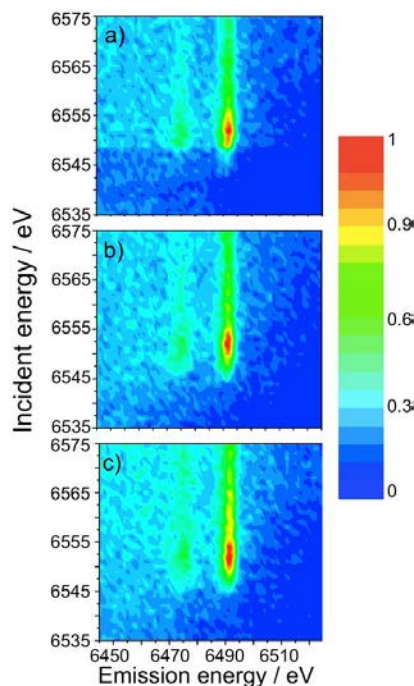


Fig. 10 RIXS maps of **2** a) in water; b) during reaction (water + H_2O_2); and c) after reaction.

Conclusions

In conclusion, we reported two novel manganese(II) complexes that show promising catalase-like properties. RIXS measurements revealed that the manganese redox chemistry is a key for the process, and the complexes are not stoichiometric catalysts, i.e., truly catalytic system. Despite being far from catalase turnover frequencies, which are among the highest of all the enzymes, the reported complexes are active in neutral aqueous conditions (physiological conditions), uncommon for catalase-mimics, making these low molecular systems a promising class of materials.

Experimental section

General remarks

$\text{MnCl}_2 \cdot 4\text{H}_2\text{O}$ and NH_4SCN were purchased from the P.O.Ch. Gliwice, 2-hydroxymethylpyridine (Aldrich, 99%), 2-(2-hydroxyethyl)pyridine (Aldrich, 99%), methanol, and $^i\text{PrOH}$ (P.O.Ch. Gliwice) were used as received.

Synthesis of the Mn(II) complexes

$[\text{Mn}_2(\mu\text{-Cl})_2(2\text{-CH}_2\text{OHpy})_4]\text{Cl}_2 \cdot 2\text{H}_2\text{O}$ (**1**)

$\text{MnCl}_2 \cdot 4\text{H}_2\text{O}$ (0.2774 g, 1.4 mmol) dissolved in 25 cm^3 of analytically pure $^i\text{PrOH}$ was added into a 25 cm^3 solution of 2-

CH₂OHpy (0.4589 g, 4.2 mmol) in ⁱPrOH. The molar ratio M:L was 1:3. The mixture was stirred for 5h and then left to crystallize at room temperature. After four weeks, light olive crystals of **1**, suitable for X-ray analysis were obtained. The product was filtered and dried under vacuum. The yield of compound **1** was about 28%. Anal. Calcd. for [Mn₂(μ-Cl)₂(2-CH₂OHpy)₄]Cl₂ · 2H₂O (C₂₄H₃₂N₄O₆Cl₄Mn₂): C, 39.78; H, 4.46; N, 7.73. Found: C, 39.74; H, 4.41; N, 7.64. IR (ν_{max}/cm⁻¹): 3388(br), 3357(br), 3206 (br), 3047(m), 3025(m), 2834(m), 1606(s), 1568(m), 1491(m), 1481(m), 1456(m), 1429(m), 1363(m), 1294(m), 1271(m), 1233(m), 1155(m), 1108(w), 1062(s), 1043(vs), 1017(s), 995(m), 971(w), 911(w), 893(w), 818(m), 785(s), 773(vs), 724(s), 686(s), 644(s), 624(s), 595(vs), 589(vs).

[Mn(2-(CH₂)₂OHpy)₂(NCS)₂] (**2**)

The complex was synthesized by reacting MnCl₂·4H₂O (0.4801 g, 2.4 mmol), 2-(CH₂)₂OHpy (0.2988 g, 2.4 mmol) and NH₄SCN (0.1850 g, 2.4 mmol) in methanolic solution. The mixture was refluxed for 1.5 h. After this time, the volume of the solvent was reduced to about 30 cm³ and the solution left out to slow evaporation. After few days, colorless crystals of the complex were obtained. The compound was filtered off and dried under vacuum box. Yield 72%. Anal. Calcd. for [Mn(2-(CH₂)₂OHpy)₂(NCS)₂] (C₁₆H₁₈N₄O₂S₂Mn) C, 46.04; H, 4.35; N, 13.42; S, 15.36. Found: C, 45.87; H, 3.96; N, 13.43; S, 14.96. IR (ν_{max}/cm⁻¹): 3223(br), 2077(vs), 1603(m), 1568(w), 1483(m), 1470(w), 1443(m), 1432(w), 1417(m), 1383(w), 1354(w), 1329(m), 1311(m), 1151(m), 1101(m), 1066(m), 1025(m), 966(w), 854(m), 785(m), 766(m), 640(m), 615(w), 594(m), 569(m), 559(m), 544(m), 536(m), 520(m), 509(m).

Methods

Chemical analysis

Elemental analysis was run on a Model Elemental Vario EL III CHN Analyzer.

Crystal structure determination

Diffraction intensity data for **1** was collected at room temperature on a KappaCCD (Nonius) diffractometer with graphite-monochromated MoK_α radiation (λ = 0.71073 Å). Corrections for Lorentz, polarization and absorption effects^{26,27} were applied. The structures were solved by direct methods using SIR-92 program package²⁸ and refined using a full-matrix least square procedure on F² using SHELXL-97²⁹. Anisotropic displacement parameters for all non-hydrogen atoms and isotropic temperature factors for hydrogen atoms were introduced.

The crystallographic measurements for **2** were performed on a Kuma KM4CCD automated four-circle diffractometer with the graphite-monochromatized MoK_α radiation. The data for the crystals were collected at 100(2) K using the Oxford Cryosystem cooler. The data were analytical corrected for absorption with the used CrysAlis RED³⁰ program. The structure was solved by direct methods using the SHELXL-97²⁹

program and refined by full-matrix least-squares methods on all F² data using the SHELXL-97²⁹ program. All non-hydrogen atoms were refined with anisotropic thermal parameters. All H atoms in **2** were found in the difference-Fourier map. H atom attached to O atom was refined with isotropic thermal parameter. Other H atoms were treated as riding with isotropic thermal parameters.

A summary of the condition for the data collection and the structure refinement parameters are given in Table 1. The figures were made using DIAMOND³¹ software. Crystallographic data (excluding structure factors) for the structure reported here have been deposited with the Cambridge Crystallographic Data Centre, as supplementary publication number CCDC 902422 (**1**), 972967 (**2**). Copies of the data can be obtained free of charge via https://www.ccdc.cam.ac.uk/services/structure_deposit/ (or from the CCDC, 12 Union Road, Cambridge CB2 1EZ, UK; fax: +44-1223-336033; e-mail: deposit@ccdc.cam.ac.uk).

Infrared (IR) analysis

Infrared (IR) spectra were recorded on a Nicolet 380 FT-IR type spectrophotometer in the spectral range 4000-500 cm⁻¹ using the ATR-diffusive reflection method.

EPR analysis

High-field, high-frequency EPR spectra were recorded during professor Julia Jezierska visit in 2011 in National High Magnetic Field Laboratory, Florida State University, Tallahassee, on a home-built spectrometer at the EPR facility of NHMFL³². X-band (9.8 GHz) were recorded on a Bruker ElexSys E500 instrument equipped with an NMR teslameter ER 036TM and a frequency counter E 41 FC (Chemistry, Wroclaw University).

Computational details

All calculations for **1** were performed with the ORCA program package³³. The program can be downloaded free of charge from <http://www.thch.uni-bonn.de/tc/orca>. The calculations were based on the X-Ray structure of **1**. The exchange integral *J* was computed at the DFT level by employing the “broken symmetry” method using the B3LYP³⁴ functional combined with Ahlrichs-type basis set TZVPP³⁴ for the Mn and Cl atoms while for all other atoms with SVP functions³⁴. The DFT calculations of ZFS were performed with the BP86³⁶ and B3LYP³⁴ functionals by using TZVPP³⁵ basis for the Mn and Zn atoms and TZVP functions³⁵ for all other atoms. For the calculations of spin-orbit (SOC) contribution to D₁, the coupled approach (CP) was used³⁷.

Thermal analysis

The thermal analyses (TG/DTG) of complexes **1**, and **2** were carried out using a TG/SDTA 851^c METTLER-TOLEDO thermobalance. The experiments were performed in nitrogen atmosphere at a heating rate of 5 °Cmin⁻¹ in the temperature range of 25–800 °C **1** and 25–1000 °C **2**, using Al₂O₃ crucible. The sample sizes are ranged in mass from 3.45 to 3.91 mg. The

thermoanalytical curves were obtained using STAR[®] System METTLER-TOLEDO software. DSC analysis for **1** was carried out using DSC METTLER-TOLEDO Instrument in standard closed sample pans, static air atmosphere, and heating rate of 5 °Cmin⁻¹.

Magnetic measurement

Magnetic measurements were carried out on a magnetic susceptibility balance (Sherwood Scientific) at room temperature by Gouy's method using Hg[Co(NCS)₄] as a calibrant.

Magnetic susceptibility data of powdered samples **1** were measured with a SQUID magnetometer (Quantum Design MPMSXL-5, Faculty of Chemistry, Wrocław University) over the temperature range 1.8–300 K at the magnetic induction of 0.5 T. Corrections for the sample holders were applied. Diamagnetic corrections for **1** were determined from Pascal's constants.

Operando resonant inelastic X-ray spectroscopy (RIXS) and catalase-like activity

The Mn K-edge RIXS maps were performed at the SuperXAS beamline at the Swiss Light Source, Paul Scherrer Institute, Switzerland. The X-ray beam delivered by the 2.9 Tesla super-cooled bending magnet was collimated by an spherically bent Rh mirror. The collimated X-rays were monochromatized by means of a double Si(111) crystal monochromator and focused by a toroidal bent Rh mirror. On the sample the photon flux was 7–8 Å⁻¹ 10¹¹ photons.s⁻¹ with an energy resolution of ΔE/E ≈ 1.4 Å⁻¹ 10⁻⁴ and a spot size of 100 μm². A 4 μm thick Mn foil was used to calibrate the energy. X-ray detection was performed using a wavelength-dispersive spectrometer, in the von Hamos geometry, which prevents scanning of components during the acquisition³⁸. The X-rays emitted from the sample were diffracted by a Ge(660) cylindrically bent crystal with a radius of curvature of 25.4 cm, and detected via a 2D Pilatus detector. The spectrometer was operated in the vertical scattering geometry.

The experiments were performed in a sealed semi-batch polyvinyl container, which was connected to a quadrupole mass spectrometer (QMS) from Hiden Analytical in order to monitor the oxygen evolution. 175 mg of the catalyst was charged into the reactor containing 20 cm³ of Milli-Q quality water, and continuously flushed with 30 cm³min⁻¹ of argon. The reaction was started, after the stabilization of the mass spectrometer, by adding 20 cm³ of H₂O₂ (30% w/w from Merck) through a spectrum with a syringe. The reaction mixture was stirred continuously to avoid beam damage, and to limit problems with mass transfer. The presented O₂ evolution profiles were corrected for QMS signal drifts with tracer (Ar m/q=36, natural abundance 0.3%), and by uncatalyzed signal, which was estimated using blank experiments (without catalyst).

Acknowledgments

The authors are specially grateful Dr A. Ożarowski (National High Magnetic Field Laboratory, Florida State University, 1800 E. Paul Dirac Drive, Tallahassee, Florida, 32310, USA) for experimental and theoretical support connected with HF EPR and DFT calculations of the dinuclear complex (**1**).

We thank the Paul Scherrer Institute for providing access to the SuperXAS (X10DA) beam line at the Swiss Light Source.

Notes and references

^aInstitute of Chemistry, Jan Kochanowski University in Kielce, 15G

Świętokrzyska Str., 25-406 Kielce, Poland. E-mail:

barbara.barszcz@ujk.edu.pl

^bPaul Scherrer Institute (PSI), 5232 Villigen, Switzerland. E-mail:

jacinto.sa@psi.ch; Tel: +41563102910

^cInstitute of Physics, Jan Kochanowski University in Kielce, 25-406 Kielce, Poland

^dFaculty of Chemistry, Jagiellonian University, 3 Ingardena Str., 30-060 Kraków, Poland

^eFaculty of Chemistry, University of Wrocław, 14 F. Joliot-Curie Str., 50-383 Wrocław, Poland

†Electronic Supplementary Information (ESI) available: Plots of J (cm⁻¹) versus various parameters. (a) J (cm⁻¹) versus the Mn–Cl–Mn angle (deg). (b) J (cm⁻¹) versus the Mn···Mn distance (Å) (Fig. S1) and TG/DTG of complex **1** (a), **2** (b), and DSC curves of complex **1** (c) (Fig. S2). See DOI: 10.1039/b000000x/

- Messerschmidt, R. Huber, T. Paulos, K. Wieghardt, *Handbook of Metalloproteins*, John Wiley and Sons Ltd., New York, 2001.
- J. A. Thomas, D. R. Morris, L. P. Hager, *J. Biol. Chem.*, 1970, **245**, 3129.
- (a) Y. Kono, I. Fridovich, *J. Biol. Chem.*, 1983, **258**, 6015; (b) W. F. Beyer Jr., I. Fridovich, *Biochemistry*, 1985, **24**, 6460.
- V. V. Barynin, P. D. Hempstead, A. A. Vagin, S. V. Lamzin, P. M. Harrison, P. J. Artymyuk, *J. Inorg. Biochem.*, 1997, **67**, 196.
- G. S. Allgood, J. J. Perry, *J. Bacteriol.*, 1986, **168**, 563.
- (a) Y. Naruta, K. Maruyama, *J. Am. Chem. Soc.*, 1991, **113**, 3595; (b) A. C. Rosenzweig, C. A. Frederick, S. J. Lippard, P. Nordlund, *Nature*, 1993, **366**, 537; (c) E. J. Larson, V. L. Pecoraro, *J. Am. Chem. Soc.*, 1991, **113**, 7809; (d) M. U. Triller, W.-Y. Hsieh, V. L. Pecoraro, A. Rompel, B. Krebs, *Inorg. Chem.*, 2002, **41**, 5544; (e) M. L. Pires dos Santos, A. Faljoni-Alário, A. S. Mangrich, A. M. da Costa Ferreira, *J. Inorg. Biochem.*, 1998, **71**, 71; (f) J. Kaizer, R. Csonka, G. Speier, M. Giorgi, M. Réglier, *J. Mol. Catal. A: Chem.*, 2005, **236**, 12; (g) J. Kaizer, T. Csay, G. Speier, M. Réglier, M. Giorgi, *Inorg. Chem. Commun.*, 2006, **9**, 1037; (h) A. J. Wu, J. E. Penner-Hahn, V. L. Pecoraro, *Chem. Rev.*, 2004, **104**, 903; (i) S. Signorella, Ch. Hureau, *Coord. Chem. Rev.*, 2012, **256**, 1229.
- A. Gacosa, R. Filiberti, *J. Canc. Prev.*, 1996, **5**, 307.
- M. Zienkiewicz, J. Szlachetko, Ch. Lothschütz, M. Hodorowicz, A. Jabłońska-Wawrzycka, J. Sá, B. Barszcz, *Dalton Trans.*, 2013, **42**, 7761.
- U. P. Singh, P. Tyagi, S. Upreti, *Polyhedron*, 2007, **26**, 3625.
- (a) E. Ember, S. Rothbart, R. Puchta, R. Eldik, *New J. Chem.*, 2009, **33**, 34; S. A. Costa, T. Tzanov, A. Paar, M. Gudelj, G. M. Gübitz, A. Cavaco-Paulo, *Enzyme Microb. Technol.*, 2001, **28**, 815.

11. (a) D.-F. Zhou, Q.-Y. Chen, Y. Qi, H.-J. Fu, Z. Li, K.-D. Zhao, J. Gao, *Inorg. Chem.*, 2011, **50**, 6929; (b) M. Nishikawa, A. Tamada, K. Hyoudou, Y. Umeyama, Y. Takahashi, Y. Kobayashi, H. Kumai, E. Ishida, F. Staud, Y. Yabe, Y. Takakura, F. Yamashita, M. Hashida, *Clin. Exp. Metastasis*, 2004, **21**, 213; (c) M. E. van Rossen, W. Sluiter, F. Bonthuis, H. Jeekel, R. I. Marquet, C. H. J. van Eijck, *Cancer Res.*, 2000, **60**, 5625; (d) M. Nishikawa, A. Tamada, H. Kumai, F. Yamashita, M. Hashida, *Int. J. Cancer*, 2002, **99**, 474.
12. N. Lah, I. Leban, *Struct. Chem.*, 2010, **21**, 263.
13. A. Jabłońska-Wawrzycka, K. Stadnicka, J. Masternak, M. Zienkiewicz, *J. Mol. Struct.*, 2012, **1012**, 97.
14. (a) J. G. Malecki, B. Machura, A. Świetlicka, T. Groń, M. Bałanda, *Polyhedron*, 2011, **30**, 746; (b) Q. Gao, Q. Bao, R. Rong, *Acta Cryst.* 2010, **E66**, m1203.
15. M. Ito, S. Onaka, *Inorg. Chim. Acta*, 2004, **357**, 1039.
16. (a) X. Song, Y. Xu, L. Li, Z. Jiang, D. Liao, *Inorg. Chem. Commun.*, 2006, **9**, 1212. (b) S. Shit, J. Chakraborty, B. Samanta, A. M. Z. Slawin, V. Gramlich, S. Mitra, *Struct. Chem.*, 2009, **20**, 633.
17. (a) D. Huang, X. Zhang, Ch. Chen, F. Chen, Q. Liu, D. Liao, L. Li, L. Sun, *Inorg. Chim. Acta*, 2004, **357**, 3295. (b) G. A. van Albada, A. Mohamadou, W. L. Driessn, R. de Gelder, S. Tanase, J. Reedijk, *Polyhedron*, 2004, **23**, 2387. (c) D. Armentano, G. de Munno, F. Guerra, J. Faus, F. Lloret, *Dalton Trans.*, 2003, **24**, 4626. (d) A. Majumder, M. Westerhausen, A. N. Kneifel, J.-P. Sutter, N. Daro, S. Mitra, *Inorg. Chim. Acta*, 2006, **359**, 3841. (e) I. I. Ebrilidze, G. Leitus, L. J. W. Shimon, Y. Wang, S. Shaik, R. Neumann, *Inorg. Chim. Acta*, 2009, **362**, 4713. (f) J.-Z. Wu, S. Tanase, E. Bouwman, J. Reedijk, A. M. Mills, A. L. Spek, *Inorg. Chim. Acta*, 2003, **351**, 278. (g) W. Zhang, J. R. Jeitler, M. M. Turnbull, Ch. P. Landee, M. Wei, R. D. Willett, *Inorg. Chim. Acta*, 1997, **256**, 183. (h) B.-K. Shin, Y. Kim, M. Kim, J. Han, *Polyhedron*, 2007, **26**, 4557. (i) M. Lubben, A. Meetsma, B. L. Feringa, *Inorg. Chim. Acta*, 1995, **230**, 169. (j) I. Romero, M. Rodríguez, A. Llobet, M. Corbella, G. Fernández, M.-N. Collomb, *Inorg. Chim. Acta*, 2005, **358**, 4459. (k) J. Rich, M. Rodríguez, I. Romero, L. Vaquer, X. Sala, A. Llobet, M. Corbella, M.-N. Collomb, X. Fontrodona, *Dalton Trans.*, 2009, **38**, 8117. (l) J.-Z. Wu, E. Bouwman, M. Mills, A. L. Spek, J. Reedijk, *Inorg. Chim. Acta*, 2004, **357**, 2694. (n) I. Romero, M.-N. Collomb, A. Deronizer, A. Llobet, J. Pécaut, L. Le Pape, J.-M. Latour, *Eur. J. Inorg. Chem.*, 2001, **1**, 69.
18. O. Kahn, *Molecular Magnetism*, VCH: New York, NY, 1993.
19. (a) J. Manzur, H. Mora, A. Vega, D. Venegas-Yazigi, M. A. Novak, J. R. Sabino, V. Paredes-García, E. Spodine, *Inorg. Chem.*, 2009, **48**, 8845. (b) D. L. Reger, A. Debreczeni, M. D. Smith, J. Jezierska, A. Ozarowski, *Inorg. Chem.*, 2012, **51**, 1068. (c) D. L. Reger, A. E. Pascui, M. D. Smith, J. Jezierska, A. Ozarowski, *Inorg. Chem.*, 2012, **51**, 11820. (d) Wei Wu, A. J. Fisher, N. M. Harrison, *Phys. Rev. B*, 2011, **84**, 024427.
20. A. Ozarowski, National High Magnetic Field Laboratory, Florida State University, 1800 E. Paul Dirac Drive, Tallahassee, Florida, 32310, USA.
21. (a) C. Duboc, M.-N. Collomb, J. Pécaut, A. Deronzier, F. Neese, *Chem. Eur. J.*, 2008, **14**, 6498. (b) L. S. Erre, G. Micera, E. Garribba, A.C. Benyei, *New J. Chem.*, 2000, **24**, 725. (c) S. Naskar, D. Mishra, S. K. Chattopadhyay, M. Corbella, A. J. Blake, *Dalton Trans.*, 2005, **14**, 2428.
22. J. Rich, C. E. Castillo, I. Romero, M. Rodriguez, C. Duboc, M.N. Collomb, *Eur. J. Inorg. Chem.*, 2010, 3658.
23. P. Glatzel, J. Yano, U. Bergmann, H. Visser, John H. Robblee, W. Gu, Frank M. F. de Groot, S. P. Cramer, V. K. Yachandra, *J. Phys. Chem. Sol.*, 2005, **66**, 2163.
24. (a) B. Hammer, J. K. Nørskov, *Nature*, 1995, **376**, 238; (b) T. Blingard, J. K. Nørskov, S. Dahl, J. Matthiesen, C. H. Christensen, J. Stheden, *J. Catal.*, 2004, **224**, 206.
25. P. Glatzel, U. Bergmann, J. Yano, H. Visser, J. H. Robblee, W. Gu, F. M. F. de Groot, G. Christou, V. L. Pecoraro, S. P. Cramer and V. K. Yavhandra, *J. Am. Chem. Soc.*, 2004, **126**, 9946.
26. Nonius COLLECT. Delft, The Netherlands: Nonius BV; 1997-2000.
27. Z. Otwinowski, W. Minor, *Processing of X-ray diffraction data collected in oscillation Methods Enzymol.*, 1997, **276**, 307.
28. A. Altomare, G. Casciarano, C. Giacovazzo, C. Guagliardi, M. C. Burla, G. Palidori, M. Camalli, *SIR92-a program for automatic solution of crystal structures by direct methods. J Appl Cryst.*, 1994, **27**, 435.
29. G. M. Scheldrick, *SHELXL-97, Program for Crystal Structure Refinement.*, University of Göttingen; Göttingen, Germany, 1997.
30. CrystAlis RED, ver. 1.171.13.66 Oxford Diffraction Poland, 1995-2003.
31. K. Brandenburg, H. Putz, Diamond-Crystal and Molecular Structure Visualization Crystal Impact, Rathausgasse 30, Bonn: GbR. 1997-2000; version 3.1f.
32. A. K. Hassan, L. A. Pardi, J. Krzystek, A. Sienkiewicz, P. Goy, M. Rohrer, L.-C. Brunel, *J. Magn. Reson.*, 2000, **142**, 300.
33. F. Neese, *ORCA – an ab initio, Density Functional and Semiempirical Program Package*, Version 2.6-35; Universität Bonn: Bonn, Germany, 2008.
34. A. D. Becke, *J. Chem. Phys.*, 1993, **98**, 1372.
35. A. Schäfer, H. Horn, R. Ahlrichs, *J. Chem. Phys.*, 1992, **97**, 2571.
36. (a) A. D. Becke, *Phys. Rev. A*, 1988, **38**, 3098. (b) J. P. Perdew, *Phys. Rev. B*, 1986, **33**, 8822.
37. F. Neese, *J. Chem. Phys.*, 2007, **127**, 164112.
38. J. Szlachetko, M. Nachtegaal, E. de Boni, M. Willmann, O. Safonova, J. Sa, G. Smolentsev, M. Szlachetko, J. A. van Bokhoven, J.-Cl. Dousse, J. Hozowska, Y. Kayser, P. Jagodzinski, A. Bergamaschi, B. Schmitt, C. David, A. Lücke, *Rev. Sci. Instrum.*, 2012, **83**, 103105.